LAWRENCE
LIVERMORE
NATIONAL
LABORATORY

LLNL-JRNL-864667

A theoretical model for sheath dynamics in the two-plasma mode of a cylindrical filament discharge

M. Sengupta, M. Campanell

May 21, 2024

Physics of Plasmas

Disclaimer

A theoretical model for sheath dynamics in the two-plasma mode of a cylindrical filament discharge

M. Sengupta[1] and M. Campanell[1, a)]
Lawrence Livermore National Laboratory, Livermore, CA 94551, USA

(Dated: 3 April 2025)

We present a refined understanding of cylindrical plasma-facing emitter cathodes by examining the limitations of the conventional space charge-limited model, which overlooks ion trapping dynamics within the virtual cathode. While conventional theory distinguishes between temperature-limited and space charge-limited regimes based on electron current constraints, our findings reveal that trapped ions can form a quasi-neutral “second plasma," expanding upstream and interacting with the primary plasma. In cylindrical, and other non-planar geometries, an expanding trapped ions layer produces current enhancement by converting more of the emitted electron flux to passing flux. The current enhancement leads to a complex coupling between the trapped-ions plasma and upstream plasma through ionizing collisions in the upstream region and charge exchange collisions in the virtual cathode. The coupling results in mutual density enhancement, and at the same time, antagonistic expansion dynamics between the two plasma layers. The process is understood using a new “Aid-Compete" model. Numerical solutions, validated against simulations, reveal the model’s capacity to predict system evolution and complex discharge behaviors, albeit with qualitative approximations.

Keywords: cylindrical hot filament discharge, ion trapping in virtual cathode, two-plasma mode, plasma coupling modeled using a set of coupled differential equations, model validation using axisymmetric particle-in-cell simulations

I. INTRODUCTION

The cathode sheath voltage plays a driving role in the properties of all laboratory plasmas generated by thermionic cathodes[1–7]. A higher plasma density can be achieved by applying a stronger bias across the cathode sheath. This accelerates emitted electrons to higher energies thereby increasing the ionization rate in the background gas . But it also leads to high ion flux and high ion impact energies on the cathode which are known to cause erosion[8]. The importance of protecting the cathode often necessitates operating at modest voltages where nonclassical sheath effects can manifest. The cathode sheath may become “space-charge limited" (SCL) where part of the emission is suppressed by a “virtual cathode" (VC) and ionization by thermoelectrons (i.e. emitted electrons) is thus reduced. Experiments and simulations have also found an “anode glow mode" (AGM) where there is a weak inverse cathode sheath and the the only ionization occurs in a thin layer of the higher-voltage inverse anode sheath[9–13].

Theoretical prediction of thermionic discharge properties[14,15] requires modeling the cathode sheath and its coupling to the plasma in the ionization region. Rigorous theories of emitting cathode sheaths exist[16] that model the classical sheath and its transition to SCL. In conventional theories, ions are presumed to propagate collisionlessly from the sheath edge to the cathode.

Recent simulation[17] and experimental[18] studies indicate that trapped ions can increase the transmitted SCL current from an emitting cathode. In a new simulation study of a cylindrical hot filament discharge, we found that the trapped ions cause more complex “aid-and-compete" dynamics within the electrode gap[19]. Specifically, the current increase caused by trapped ions proportionally increases the ionization rate in the upstream plasma. Yet at the same time, the trapped ion region forms a second quasineutral plasma that reduces the space available to the upstream plasma. Either plasma can take over the electrode gap and expel the other as the discharge evolves. Improved theoretical understanding of the dynamics is needed to explain how the single-plasma and two-plasma discharge modes form and how they will evolve as operating conditions are changed.

The purpose of this paper is to provide a formal theoretical foundation for the dynamics of a thermionic discharge that includes trapped ion effects and explains the transitions among classical, SCL, and inverse sheath modes[10,20–24]. Because thermionic cathodes often take the form of wire filaments[25–27] or rods[18] we will treat the example of a cylindrical geometry discharge between a small inner emitting cathode and a concentric outer anode. We will find that the model is able to explain some dynamical effects observed in our fully kinetic simulation study[19] at comparatively negligible computational cost. A more complete quantitative agreement would require further refinement of the model and lifting some simplifications that were invoked to make the equations more tractable. This paper is intended to serve as a starting point that can be built upon in future work. The main concepts introduced here, especially how the two plasma regions couple to each other, are adaptable to other electrode arrangements.

In Section II, we outline the foundations of the aid-and-compete model and derive the model equations. In Section III, we calculate solutions of the equations and compare with fully kinetic simulations. Section IV gives concluding remarks and suggestions for future enhancements of the model.

[a)]Corresponding Author; Electronic mail: sengupta4@llnl.gov

II. THE AID-COMPETE MODEL FOR DYNAMICS IN THE TWO-PLASMA-MODE OF A DISCHARGE

In a recent simulation study of a cylindrical filament discharge we demonstrated that operating the discharge within a small window of voltage bias in the range ~ 1–$2V$ above the ionization threshold of the working gas, allowed the discharge to evolve unconventionally revealing new dynamics such as sheath mode transitions, current enhancement, and hysteresis[19]. The reason for this was found to be the formation of a trapped-ions layer in the potential well of the discharge's virtual cathode, a process that can only be sustained in this range of voltage bias. Higher voltage biases generally tend to make the ionization of the working gas too rapid such that the Virtual Cathode (VC) has to give way to a classical (ion-rich) sheath at the filament, taking the discharge to what is called the Temperature Limited Mode or TLM. At biases lower than the ionization threshold, no quasi-neutral plasma can be sustained.

Only close to the ionization threshold, a layer of quasi-neutral plasma forms in the region of the VC made up of trapped ions and emitted electrons. The cathode-wards accelerating ions get trapped in the VC, when they happen to make de-energizing charge exchange collisions with background neutrals in the VC. The formation of a trapped ions layer modifies the potential structure of the VC giving it an extended minimum. We call this layer the Trapped Ions plasma (TIP). The TIP interacts with the upstream plasma layer that is formed by the conventional impact ionization process. In this configuration where we have two plasma layers occupying the upstream and downstream regions of the electrode gap, the applied bias gets dropped for the most part, in a Double Layer (DL) formed between the TIP and the upstream plasma. We call this mode of discharge the Two Plasma Mode (TPM)[19].

The TPM configuration shares both morphological and operational similarities with another multi-sheath solution, the plasma fireball[28]. Both TPM and fireballs feature a double layer connecting a second quasi-neutral layer— formed near an electrode— to the conventionally formed plasma layer[29]. Additionally, both exhibit hysteresis under certain electrode bias modulations[30].

However, it is important to note that TPM and fireballs are fundamentally different phenomena. Anodic double-layer solutions, such as fireballs, form due to enhanced electron impact ionization near the anode. In contrast, the two plasma mode arises from a trapped-ion layer near an emitting cathode, driven by ion trapping dynamics facilitated by charge exchange collisions.

With build up of more trapped ions, the VC gets flatter due to neutralization of electron space charge, and wider due to the expansion of the the TIP. The stretching of the VC minimum due to an expanding TIP has been observed in both planar[12] and non-planar discharges[31], but unlike planar electrodes, in non-planar electrodes such as cylindrical or spherical, the TIP's expansion causes an enhancement of the space charge limited current in the discharge. The effect can be understood by conventional Space Charge Limited (SCL) sheath theory. At the junction between the modified VC and the DL, the potential has a Marginal SCL or MSCL structure, a shape than can be considered a boundary between an SCL and a classical sheath. Using theory of MSCL sheath[16] we will demonstrate in this paper, than for a given discharge system, the electron current density emanating from the MSCL becomes fixed by the system parameters. This implies that as the TIP expands upstream to higher radius the MSCL current density it transmits into the DL will remain conserved. Hence in the axisymmetric configuration of a cylindrical filament discharge, the electron current has to increase in proportion to $r_v(t)$, the dynamic radial width of the TIP / modified VC. The expanding TIP draws more electrons from the emitted flux and transmits them across into the passing flux of the electrode. So in effect, the SCL current is increased due to the increasing fraction of passing to emitted electrons.

In the appendix of Ref.[19] we demonstrated using simulation that in cylindrical geometry an expanding TIP produces a current that grows in proportion to the increasing radial width of the TIP. It was also demonstrated in Ref [19] that the rise in current hits a limit when the passing electron flux becomes equal to the emitted electron flux, at which point the modified VC is affected by a violent quenching instability that ejects all trapped ions into the cathode and reforms a regular VC with a unique minimum; only for the ion-trapping process to start again.

The electron current enhancement by a radially expanding TIP sets forth a coupling mechanism between the TIP and the upstream plasma. The increased electron flux leads to more ionization in the upstream plasma increasing its density. More ions from the upstream plasma are now transmitted downstream across the DL into the modified VC. This leads to more ion-trapping and growth of the TIP. This feedback mechanism of mutual growth between the TIP and the upstream plasma layers also causes the two plasma layers to expand into the electrode gap approaching each other in the process. The expansion dynamics is antagonistic, where the stronger expansion of one layer within the limited electrode gap, can cause the other layer to shrink. The combined effect of the mutual enhancement and antagonistic expansion of the two plasmas is referred as the "aid-compete" effect[19].

The aid-compete model offers a way of understanding the coupling between the trapped-ions plasma and the upstream plasma in the two-plasma mode (TPM) of a cylindrical coaxial discharge. In the name of the model, the 'aid' part refers to the coupling mechanism that produces mutual density enhancement of the two plasma layers. The 'compete' part refers to the antagonistic expansion dynamics of the two plasma layers in the electrode gap. In Ref.[19] we explained and demonstrated the aid-compete effect using simulations of the two-plasma mode of a cylindrical filament discharge. In this paper we will derive an approximate analytical form of the model and compare its solutions for some given parameters with corresponding simulations. It will be revealed that the simulations grossly agree with the model, indicating that our model incorporates the essential coupling mechanisms between the two plasma. At the same, divergence between simulation data and the model at a finer level, leaves scope for refinement of the model to make it more predictive which will

be discussed.

The analytical form of the aid-compete model should be treated as the first attempt to mathematically grasp the dynamic, nonlinear, collisional coupling mechanism between the TIP and upstream plasma, leaving some allowance for inexact convergence with the simulations. To build the model we first understand the unconventional two-plasma mode of a discharge in the following subsection.

A. The Two Plasma Mode or TPM

In Fig. 1, a snapshot from simulation[19], we observe the TPM. In the system, the inner cathode is biased to $V_B = -17V$ while the outer anode is grounded. R_{ct} and R_{an} on the radial axis of Fig.1 represent the cathode and anode boundaries. The potential, Φ, reveals a distinct behavior across the radial domain. It decreases sharply from the cathode in a thin inverse sheath before stabilizing into a quasi-neutral area of nearly flat potential in the trapped-ions plasma. Exiting the upstream side of the trapped-ions plasma, the potential forms a Marginal-Space-Charge Limited (MSCL) sheath, with Φ increasing radially towards the upstream plasma potential in a charge-accelerating double-layer. The radial increase in Φ saturates in the upstream plasma region, delineating the second region of nearly flat potential. Approaching the anode, Φ decreases to match the anode's fixed potential, forming a classical sheath. The voltage across the accelerating double layer region is equivalent to the applied bias plus an additional $0.6V$ in this snapshot, due to the influence of the electrode sheaths on the interior potential.

The corresponding electron and ion densities n_e and n_i clearly depict that - (i) the cathode sheath region has more electrons than ions hence the inverse sheath of Φ (see Fig.1-inset (I)) , (ii) the trapped-ions plasma is quasi-neutral and has an almost flat potential, (ii) the double-layer transits from electron rich to ion rich as Φ rises in the acceleration region (see Fig.1-inset (II)), (iv) the upstream plasma is quasi-neutral with weak potential gradients, and (v) the anode sheath has more ions than electrons, hence a classical sheath (see Fig.1-inset (III)).

In the TPM, the emitted electrons that enter the double layer get accelerated to ionizing energies producing an upstream plasma through electron impact ionization of neutrals. Ions from the upstream plasma are transported downstream via the same double layer. In their trajectory towards the cathode, some ions would make charge exchange collisions with cold neutrals residing in the Virtual Cathode (VC), producing cold ions that are captured within the potential well of the VC. The accumulated trapped ions within the VC form a second layer of plasma that is neutralized by the portion of emitted electrons that get past the thin inverse sheath.

The TPM can be thought of as the general solution for all the four sheath modes of the thermionic discharge. The single-plasma modes (see Fig.1 of Ref.[19]) can be obtained as limiting cases of the TPM when the radial width of one of the plasma layers approaches zero. If the trapped ion plasma's width reduces to zero, the discharge will either be in the familiar classical sheath "temperature-limited mode" (TLM) or in a SCL sheath mode without trapped ions, also known as the "Langmuir mode" (LM), see Fig. 4 of Ref.20. On the other hand, if the upstream plasma width reduces to zero and the trapped ion plasma takes over, the discharge is in the "Anode Glow Mode" (AGM). Our simulation studies suggest that discharges have a strong tendency to settle to a one-plasma steady state rather than a TPM. But understanding the TPM is crucial because the TPM often forms during the initial striking of a discharge, or after a single-plasma discharge is subjected to an adjustment of operating conditions similar to what would happen in an experiment. In all cases, the aid-and-compete dynamics between the two plasmas determines which steady state modes are accessible in which regions of operating parameter space.

We proceed to formulate the aid-compete model.

B. An overview of the set of equations that form the aid-compete model

As demonstrated in Ref.[19] the feedback process of mutual density growth in the TIP and the upstream plasma, and their antagonistic spatial expansions to occupy the electrode gap act in unison. In combination, these processes dynamically evolve the densities of the two plasma layers and their radial widths in the gap. In our model we represent the changing densities of the two plasma layers with the functions $\frac{dP_{ups}}{dt}$ and $\frac{dP_{trp}}{dt}$ where P_{ups} and P_{trp} represent the total spatially integrated population of the upstream plasma and the trapped-ions plasma respectively, see Fig.1. We represent the movement of the two plasma layers, using a common variable r_v (subscript 'v' used to represent a variable radius). Technically r_v is the radial extent of the modified virtual cathode or TIP. The remaining space in the radial domain, which is occupied by the double layer plus the upstream plasma (see Fig.1), is taken as a rough approximation for the width our model's 'upstream plasma' with population P_{up}. The width of the thin inverse cathode sheath and the classical anode sheath in Fig.1 is neglected in our model. The resulting picture of the density profile is schematically represented in the top panel of Fig.2. The grey and yellow regions are quasi-neutral and they represent P_{trp} and P_{ups} respectively. The two quasi-neutral populations are separated by an operational boundary at $r = r_v$.

The movement of $P_{up}(t)$, $P_{trp}(t)$ and $r_v(t)$ is the solution from the model. For example, a sheath transition where the trapped ions plasma grows in density and radially expands, while the upstream shrinks[19] will be represented in our solution by increasing P_{trp} and r_v and a decreasing P_{ups}.

The quasi-neutral density functions of the TIP and the upstream plasma are assumed to be purely geometric, hence $\propto 1/r$, as indicated in Fig.2 - top panel. In Fig.2 we have shown sheaths of finite widths at the cathode and anode for the purpose of understanding the model. In application of the model these widths are neglected as mentioned earlier. Hence the left bounding density of the TIP, n^L_{trp} is approximated to be at the cathode's radius, R_{ct} (see Fig.1) while its right bounding value, n^R_{trp} is at the operational boundary at $r = r_v$. The

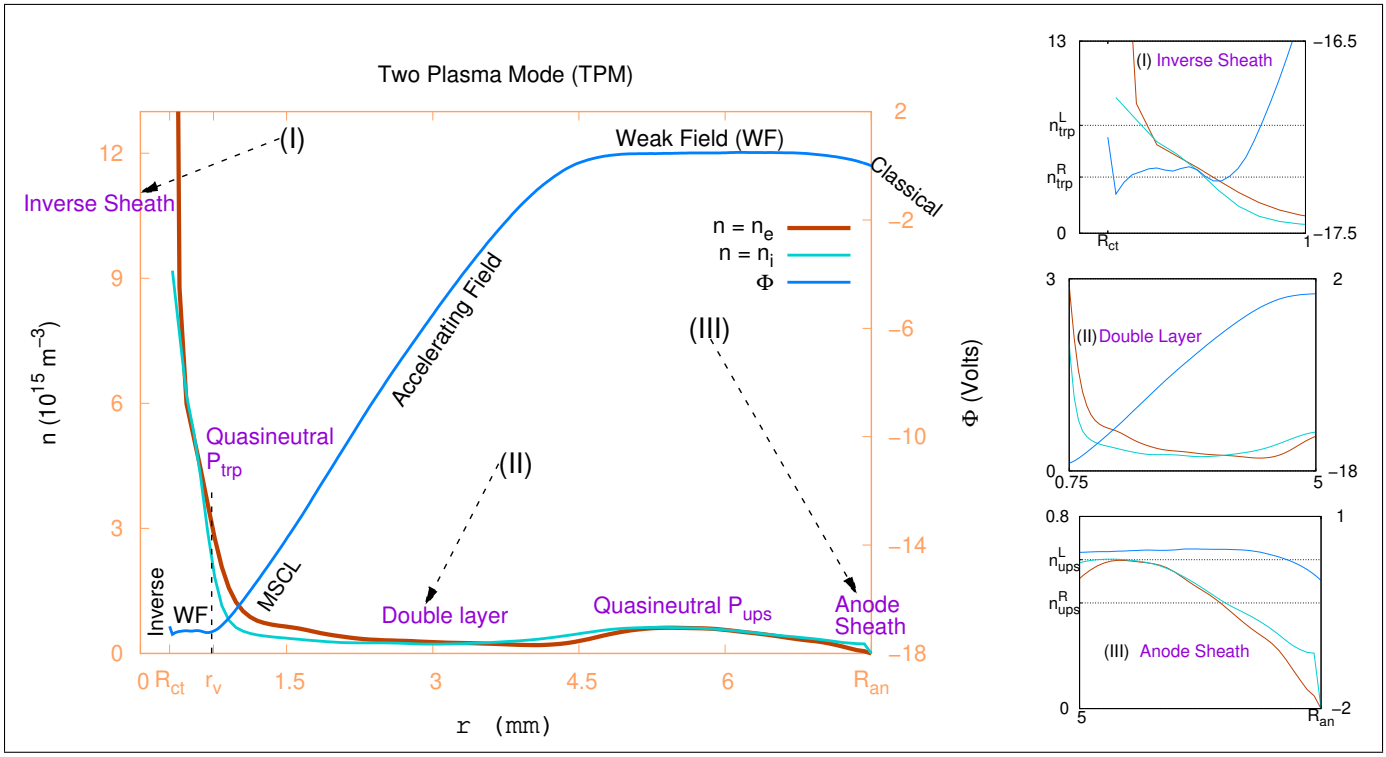

FIG. 1: The two plasma mode (TPM): A snapshot from simulation is used for illustration. The graph is dual, showing the electron density n_e and ion density n_i on the left y-axis and the potential function Φ on the right y-axis. Distinct regions on the potential profiles are labelled in black. Different discharge regions are marked in magenta along the density profile. P_{trp} and P_{ups} are the quasi-neutral populations (i.e. total amount of plasma) of the trapped-ions plasma and the upstream plasma. R_{ct} and R_{an} on the radial axis show the position of the cathode and anode respectively. The radial extent of the trapped-ions layer is demarcated as r_v on the radial axis. 'WF' implies a weak field region and 'MSCL' refers to a marginal space charge limited sheath. Inset (I) is a zoomed-in plot of the inverse cathode sheath and trapped-ions layer where n^L_{trp} and n^R_{trp} marks the downstream and upstream quasi-neutral density of the trapped-ions layer. Inset (II) is a zoomed-in plot of the double layer. Inset (III) is a zoomed in plot of the classical anode sheath where n^L_{ups} and n^R_{ups} mark the downstream and upstream quasi-neutral density of the upstream plasma. Note that the snapshot shown here was chosen for clarity of the different regions of the discharge. The double layer is not always so wide.

density decreases as $1/r$ between the two boundaries. Similarly the upstream plasma's density function starts from its Left boundary at radius r_v with a density value n^L_{ups} and falls smoothly as $1/r$ up to its Right boundary at $\approx R_{an}$ where its value is n^R_{ups}. In our model, a density jump occurs at location r_v because the plasma densities on either side of the DL are unequal: n^R_{trp} on the downstream side and n^L_{ups} on the upstream side. The location r_v acts as an operational boundary, where the $n^R_{trp}(r_v)$ and $n^L_{ups}(r_v)$ are related through the theory of Marginal Space Charge Limited (MSCL) sheaths[16].

An important quantity indicated on the density axis of Fig.2 - top panel is the fixed emission density n_{emt} on the cathode filament. As depicted in Fig.2 the actual density of electrons on the filament can exceed n_{emt} because of reflected electrons by the space charge. We assume an exponential Boltzmann decay of n_{emt} to the left boundary value of the TIP-density, n^L_{trp}. The Boltzmann decay is indicated by the thick black dashed curve in the top panel of Fig.2. This relation follows from an approximation that at the density value n^L_{trp} the electron distribution has no reflected electrons left i.e. all the electrons at this point are headed radially outwards.

The bottom panel of Fig.2 represents the assumed potential function in our model. Important flux quantities are also represented using broad arrows. These include the fixed emitted electron flux Γ_{emt}, and the transmitted or passing flux Γ_{tmt}. The Γ_{emt} is the emergent electron flux through the inverse sheath at the cathode formed by space charge electrons, see Fig.1. The inverse sheath imposes a potential barrier of strength $-\Phi_{bar}$ on the emitted electrons, suppressing the Γ_{emt} to Γ_{tmt} as represented in the bottom panel of Fig.2. In our model the $-\Phi_{bar}$ and the Γ_{tmt} are dynamic quantities.

Another important flux quantity shown in Fig.2 - bottom panel is the downstream ion flux of the Bohm kind from the upstream plasma. This flux provides the ions for trapping the virtual cathode. In our model the upstream Γ_{tmt} and the downstream Bohm flux are assumed to be conserved across the operational boundary. However electrons and ions are assumed to gain energy equal to the voltage difference of the double

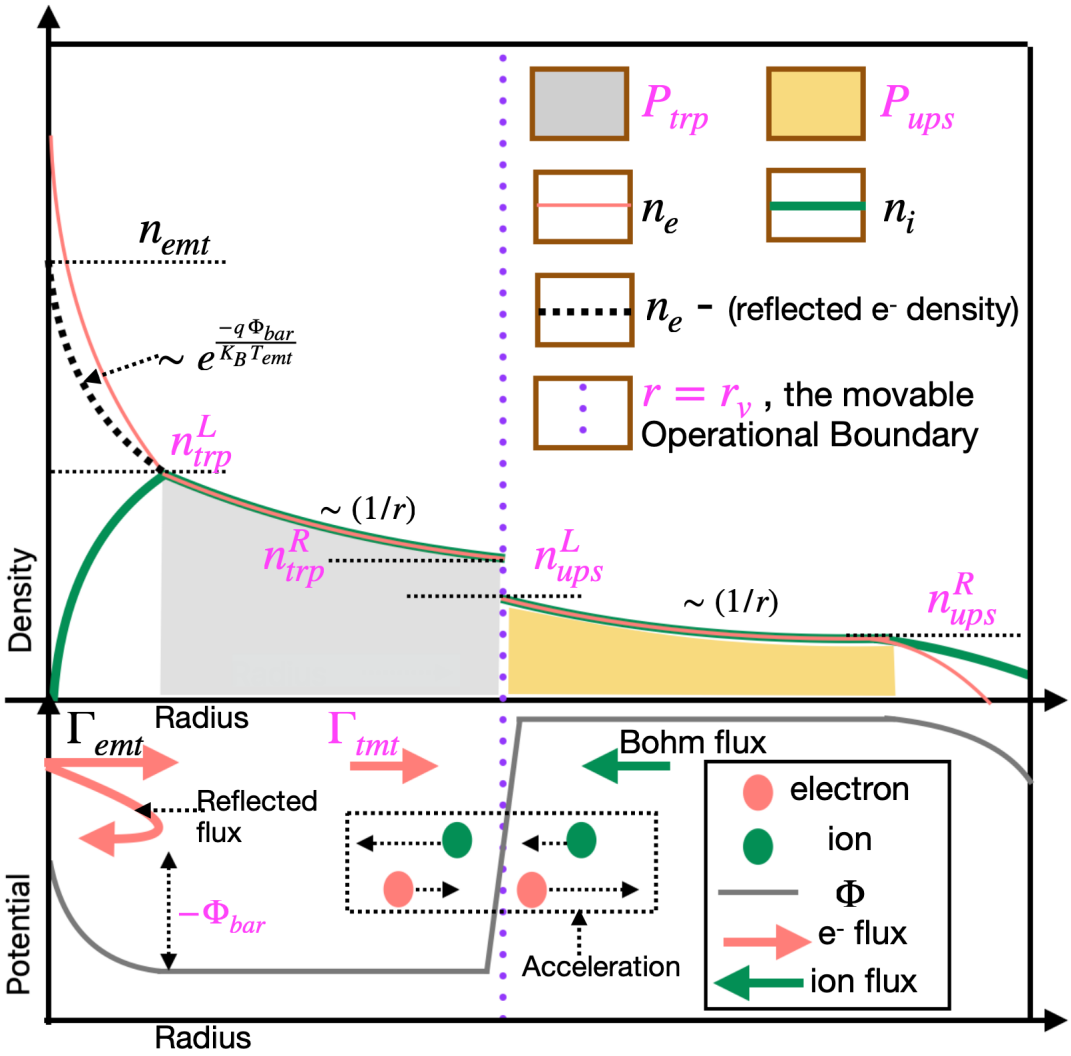

FIG. 2: A schematic representation of the aid-compete effect in the two plasma mode of a cylindrical discharge. The top plot represents the assumed analytical shapes of the radial density functions for electrons and ions in different regions of the discharge. The bottom plot represents the corresponding assumed shape of the radial potential function. Important quantities and effects are symbolically represented on the figure to be taken up in the corresponding discussion. The solved variables are distinguished using magenta print.

layer (see Fig.1) upon crossing the operational boundary in opposite directions. This acceleration is also schematically represented in the bottom panel of Fig.2. The implication for the numerical works of the model is as follows. We use Γ_{tmt} for the number of electrons entering the upstream plasma in unit time. The energies of these electrons used to calculate the mean free path of ionization, Δ_{iz}, is the accelerated energy past the operational boundary. Similarly the number of ions entering the TIP per unit time is the calculated Bohm flux and the ion energy used to calculate the mean free path for charge exchanges in the TIP, Δ_{cx} is the accelerated ion energy past the operational boundary.

The analytical model solves for the rate of change of the upstream and downstream populations, $\frac{dP_{ups}}{dt}$ and $\frac{dP_{trp}}{dt}$ using a pair of coupled differential equations, the equations 1 and 2 in the following subsection. The multiple variables that feature in this two differential equations, are systematically reduced to a solvable pair of variables using algebraic relations derived from standard theory of sheaths, the Eq.s 3-9 in the following subsections. In Fig.2 the 9 solved variables viz. P_{trp}, P_{ups}, r_v, n^L_{trp}, n^R_{trp}, n^L_{ups}, n^R_{ups}, Γ_{tmt}, $-\Phi_{bar}$ are distinguished using magenta print. Remaining constant values that appear in the set of equations 1-9 include (i) the temperature T_{emt} of the emitted electrons (ii) T_e the (assumed) electron temperature of the upstream plasma, (iii) T_i the (assumed) common temperature of ions in the upstream plasma and trapped-ions plasma, (iv) α a proportionality constant that will be calculated using MSCL sheath theory[16], and (v) the physical constants for electron mass m_e, ion mass m_i, Boltzmann constant k_B, and electron charge magnitude q.

C. Derivation of the equations of the aid-compete model

We start with the equation describing the rate of change of the upstream plasma population, P_{ups}.

$$\frac{dP_{ups}}{dt} = \Gamma_{tmt}\left(1-\mathrm{e}^{-\frac{(R_{an}-r_v)}{\Delta_{iz}}}\right) -2\pi R_{an} n^R_{ups}\sqrt{\frac{k_B T_e}{m_i}} -2\pi r_v n^L_{ups}\sqrt{\frac{k_B T_e}{m_i}} \tag{1}$$

The first term on the right hand side (RHS) of Eq.1 calculates the rate of electron impact ionization. Here Γ_{tmt} represents the transmitted electron flux (not flux density) - the portion of the injected electron flux Γ_{emt} that makes it past the space charge voltage barrier, $-\Phi_{bar}$ of the inverse cathode sheath. It is approximated in our model that these electrons propagate collisionlessly through the quasi-neutral space of the trapped-ions plasma, and then get accelerated by the double layer to an energy sufficient to cause ionization of neutrals. The factor in parenthesis is the probability of each accelerated electron causing an ionization, which is expressed in terms of an ionization mean free path Δ_{iz} and the length of the upstream plasma, $R_{an}-r_v$.

The upstream plasma's length is $R_{an}-r_v$ in our model, neglecting for simplicity, the space consumed by the Double Layer (DL). This approximation comes from a simplifying 'small Debye length' assumption that we apply for all the sheaths in the TPM - cathode, anode, and DL. However, as the simulation snapshot Fig.1 shows us, the DL does not necessarily have a negligible width compared to the plasma widths. Because the DL's width is coupled in time to both plasmas, including it in the equations would introduce entanglements that make them considerably more complicated to solve. We trade off the DL width for tractability of our model.

To estimate the constant Δ_{iz}, one can approximate that the energy of accelerated electrons is comparable to the mean initial energy of thermoelectrons, E_{th}, plus the electrode bias voltage and use the known ionization cross section of the gas at that energy[32,33]. The actual accelerating voltage in the double layer is larger than the applied bias $|V_B|$ by some voltage δV. The δV accounts for the sum of the inverse cathode sheath and classical anode sheath voltage magnitudes; see Fig.1. We neglect time variation of the sheath voltages. The Δ_{iz} is calculated using the ionization cross-section $\sigma_{iz}(E_{th}+q|V_B|+q\delta V)$.

Another simplification in the theory is neglecting the role of elastic scattering and energy-loss excitation collisions on the thermionic beam. The effects of non-ionizing collisions on the predicted ionization rate is expected to be negligible because the mean free paths of all types of electron collisions are much longer than the electrode gap radius in the pressure range under consideration for the TPM ($\sim 25\,mTorr$). Higher neutral pressures generally tend to produce TLM.

The second and third terms on the RHS of Eq.1 represent the loss of plasma (estimated via Bohm's criterion on ions) from the two radial bounds of the upstream plasma with local densities n^L_{ups} and n^R_{ups}. The term with R_{an} represents losses to the anode while the term with r_v represents losses from the upstream plasma towards the cathode. T_e is the known electron temperature in the upstream plasma.

Next we calculate the rate of change of the trapped ions plasma population, P_{trp}.

$$\frac{dP_{trp}}{dt} = 2\pi r_v n^L_{ups}\sqrt{\frac{k_B T_e}{m_i}}\left(1-\mathrm{e}^{-\frac{(r_v-R_{ct})}{\Delta_{cx}}}\right) -2\pi R_{ct} n^L_{trp}\sqrt{\frac{k_B T_i}{2\pi m_i}}\mathrm{e}^{-\frac{q\Phi_{bar}}{k_B T_i}} \tag{2}$$

The first term on the RHS of Eq.2 represents the creation of trapped ions. Ions from the upstream plasma are assumed to enter the potential well of the Virtual Cathode (VC) at a rate associated with the Bohm criterion $-2\pi r_v n^L_{ups}\sqrt{\frac{k_B T_e}{m_i}}$, same as the downstream loss term in Eq.1. The factor in parenthesis estimates the probability of a charge exchange collision for each ion passing through. This probability is expressible in terms of the radial width $(r_v - R_{ct})$ of the Trapped Ions Plasma (TIP) and Δ_{cx}, the mean free path of charge exchange collisions. Assuming that the ions are accelerated from negligible initial energy to $|V_B|+\delta V$ across the DL we can calculate Δ_{cx} by estimating the charge exchange cross-section[32,34], $\sigma_{cx}(q|V_B|+q\delta V)$.

The second term on the RHS of Eq. 2 represents the loss rate of trapped ions escaping to the cathode over a potential barrier of height Φ_{bar} formed by the inverse sheath; see Fig.1. We assume that the trapped ions are singly charged and are Maxwellian at the sheath edge with constant temperature T_i and variable density n^L_{trp}. Trapped ions in practice might be expected to be in a collisional thermal equilibrium (and hence Maxwellian) with the background neutrals at room temperature $< 0.03\,eV$. But the trapped ions tend to acquire additional energy through collisions with thermoelectrons or the effects of instabilities. A typical T_i measured from simulations[19] is $\sim 0.1\,eV$. No trapped ions have sufficient energy to escape through the upstream side over the immense double layer's barrier $\sim |qV_b| \gg k_B T_i$.

Having established the two main differential equations Eq.1 and 2 we proceed to derive some algebraic relations between the 9 unknown quantities in Eq.1 and 2 which would help in reducing the total number of unknowns to two, making Eq.1 and 2 solvable.

To establish a system of equations with a finite number of unknowns, we make informed assumptions about the radial charge distribution in both plasma regions. This will help us link the values of P_{ups} and P_{trp} to the local densities at the plasma boundaries. Plasma density upstream will develop at a rate proportional to the flux density of the accelerated thermionic beam which in the cylindrical axisymmetric discharge has a $1/r$ distribution as long as collisionality is low, meaning that the attenuation of the beam is weak across the electrode gap. We will therefore approximate that the upstream plasma has a $1/r$ spatial density distribution. This ignores the effects of plasma force balance and presheath physics on the upstream density distribution which

are too complicated to embed in the analytical model. Simulations suggest that a density assumption, $n(r) \propto 1/r$ is roughly reasonable[19]. The amount of plasma particles at each r (azimuthally integrated) is then $\propto \frac{2\pi r dr}{r}$, independent of r. The cumulative (radially integrated) amount of plasma upstream P_{ups} can then be expressed in terms of n^L_{ups} and r_v via the relation -

$$P_{ups} = 2\pi r_v n^L_{ups} (R_{an} - r_v) \tag{3}$$

We also approximate that the trapped ion plasma has a $1/r$ density distribution within its bounds, resulting in a similar expression for P_{trp}.

$$P_{trp} = 2\pi R_{ct} n^L_{trp} (r_v - R_{ct}) \tag{4}$$

This justification is more intricate. Because the trapped ion region has roughly zero electric field, the emitted electrons passing through expand radially and (ignoring collisions) must have a $1/r$ spatial density distribution, and thus so do the neutralizing trapped ions. This argument holds even if the creation of new trapped ions follows a different radial distribution. For example, if the mean free path of charge-exchange collisions is smaller than the radial length of the trapped ion plasma, which sometimes occurs in simulations, most trapped ions will be created near the outer bound of the region. Experience with simulations shows that weak electric fields will establish to move the trapped ions closer to the cathode to set up the approximate $1/r$ density profile. Incidentally, we note that there will always be some un-collided, high-energy ions passing through the trapped ion region, but their spatial density is comparatively small and has been neglected.

The relation between the emitted electron flux from the cathode, Γ_{emt} and the electron flux transmitted through the inverse sheath, Γ_{tmt} is expressed in analytical form as-

$$\Gamma_{tmt} = \Gamma_{emt}\, e^{-\frac{q\Phi_{bar}}{k_B T_{emt}}} \tag{5}$$

The two fluxes are connected by an exponential factor which represents the Boltzmann decay in electron density across the $-\Phi_{bar}$ inverse sheath. Cylindrical decay of thermoelectron density within the inverse sheath was neglected in Eq.5 under the approximation of zero sheath thickness. The electrostatic decay of the emitted electron density is much more pronounced than its geometric decay.

For a half-Maxwellian emitted electron population with known flux density Γ_{emt} and temperature T_{emt} their density at the cathode n_{emt} is also known. The inverse sheath barrier attenuates the $+r$ flux and the density electrostatically (not geometrically) by the same factor. Eq.6 is a resulting relation that links variable values n^L_{trp} and Γ_{tmt} at the downstream edge of the trapped ion plasma to known values at the surface.

$$\frac{n_{emt}}{\Gamma_{emt}} = \frac{n^L_{trp}}{\Gamma_{tmt}} \tag{6}$$

Using the known Γ_{emt} and the mean radially directed velocity, $v_{inj} = \sqrt{\frac{2k_B T_{emt}}{\pi m_e}}$ (m_e is electron mass), we can get an approximate value for n_{emt} using the relation $\Gamma_{emt} = 2\pi R_{ct} n_{emt} v_{inj}$. We note that the actual density of electrons at the cathode can be higher than n_{emt} due to those reflected by the inverse sheath.

Next, the downstream and upstream densities of the trapped-ions plasma, n^L_{trp} and n^R_{trp} are connected based on the previously discussed $1/r$ (geometric decay) radial density profile.

$$n^L_{trp} R_{ct} = n^R_{trp} r_v \tag{7}$$

Eq.8 relates the upstream density of the trapped-ions plasma n^R_{trp} with the downstream density of the upstream plasma, n^L_{ups}.

$$n^R_{trp} = \alpha\, n^L_{ups} \sqrt{\frac{\pi m_e}{2k_B T_{emt}}} \tag{8}$$

The n^R_{trp} and n^L_{ups} quantities are interconnected because the double layer between them must maintain the structure of a “marginal SCL" (MSCL) sheath as the two plasmas evolve in time. For calculation tractability, we approximate that the MSCL sheath is thin enough to exhibit local planar geometry even though its radial extent in simulations is often wider. In planar sheath theory[16], the emitted electron flux density through a MSCL sheath Γ_{MSCL} is proportional to the density of the plasma at the upstream sheath edge. Let us define α as the proportionality coefficient, $\Gamma_{MSCL} = \alpha n^L_{ups}$. Then using the fact that in our system the Γ_{MSCL} is the product of spatial density of the thermoelectrons entering the double layer, n^R_{trp}, and the known thermoelectron thermal velocity, we arrive at Eq.8. The value of α can be estimated using existing models of MSCL sheaths[16].

As an alternate to using the theory of MSCL sheaths[16] to establish a relationship between n^R_{trp} and n^L_{ups} one could also apply the Langmuir condition[35,36] for the current across the Double Layer (DL). The Langmuir condition for double layer states that the ratio of the electron flux to the ion flux across the DL is equal to $\sqrt{(m_i/m_e)}$. Imposing the Langmuir condition on our system we get the relation $n^R_{trp} v_{inj} = \sqrt{(k_B T_e/m_e)}\, n^L_{ups}$, where the term $\sqrt{k_B T_e/m_e}$ mimics the role of α in Eq.8. For our system the value $\sqrt{k_B T_e/m_e} = 7.24 \times 10^5\, ms^{-1}$ is comparable to estimated value of the α function, $\alpha = 8.25 \times 10^5\, ms^{-1}$ obtained from MSCL sheath theory[16]. However the two relations are not exactly equivalent. The Langmuir condition[35,36] is arrived at by assuming counter-propagating ion and electron beams emitted at zero velocity from opposite boundaries. A plasma-facing thermionic cathode sheath as modelled by Takamura et al[16] has several additional complexities including (a) a confined plasma electron species contributing to the space charge distribution in the sheath, (b) a substantial ion injection velocity given by the Bohm criterion, (c) nonzero emitted electron temperature, and

(d) quasineutrality among the plasma electron, emitted electron and ion charge populations is imposed at the ion-injection boundary.

Interestingly upon closer examination, the two models seem to approach each other under certain conditions, in particular, a very large voltage bias reaching tens of T_e. This looks consistent with intuition on the grounds that under large bias, finite injection velocities of emitted electrons and ions would become negligible and the plasma electrons have negligible penetration into the sheath. Such extreme biases are generally not usable due to practical considerations such as ion sputtering. So to keep our result general and valid for the full range of biases, we opt to express the MSCL current in terms of Takamura's cathode sheath model[16].

Finally, Eq.9 relates the density at the inner and outer boundaries of the upstream plasma $n^L_{ups}$and n^R_{ups} based on the presumed $1/r$ (geometric decay) spatial density profile.

$$n^L_{ups}\, r_v = n^R_{ups} R_{an} \tag{9}$$

D. Visualizing the model at work through the equations

The set of Equations 1-9 gives a feel of the aid–compete effect that will be at work when they are solved together. For example, the first term on the RHS of Eq. 2 which feeds ions to the trapped-ions plasma has a coefficient that is proportional to the upstream plasma's population through n^L_{ups}. Hence as P_{ups} builds in Eq. 1 it will aid the growth of the downstream plasma through Eq. 2.

Again, From Eq.5 and 6 we have-

$$-\Phi_{bar} = \frac{k_B T_{emt}}{q} \ln\left(\frac{n^L_{trp}}{n_{emt}}\right) \tag{10}$$

In Eq.10 the logarithmic term is negative as $n^L_{trp} \leq n_{emt}$. As n^L_{trp} approaches n_{emt} through more and more ion trapping in Eq.2, the barrier height Φ_{bar} will approach zero. This will lead to an increase of Γ_{tmt} through Eq.5 which will in turn feed the ionization term in Eq.1 aiding the growth of the upstream plasma.

A compete effect between the plasmas occurs because any increase in the radial length of one plasma reduces the other's. Meanwhile, the particle gain terms of Eqs.1 and 2 indicate that the creation rate of new ions in each plasma is an increasing function of its existing length. Thus, movement of r_v in either direction can feedback on itself, favoring the expanding plasma to take over. That outcome is not guaranteed, however. Data will show that r_v can be moving in one direction and then turn around, in some calculations. The length of one plasma can be decreasing even while its total content P_{ups} or P_{trp} is increasing, and vice versa. Equilibrium TPM's are even possible in principle. But they have not yet been observed in our simulations[19] or model calculations. The reason, we argue, is that it is improbable for two plasmas to simultaneously achieve a balance with exactly equal particle creation and loss rates within.

It is worthwhile to discuss how the discharge model changes if trapped ions are not considered. Maintaining the assumption of thin planar space charge sheaths for simplicity, conventional theories of a filament with a thin SCL sheath would predict the MSCL current *density* to be transmitted past the virtual cathode at all points around the cathode surface. With a trapped ion plasma in the VC, its outer edge transmits the MSCL current *density*, so having an $r_v > R_{ct}$ enhances the total amount of current emitted from the filament cathode by a factor r_v/R_{ct} in cylindrical geometry. This current enhancement is produced via a reduction of the barrier height Φ_{bar} which electrostatically (not geometrically) regulates the portion of the emitted electron flux allowed to enter the TIP. The trapped ion plasma is eliminated in our model when r_v reaches R_{ct}. In this scenario, $n^L_{trp} = n^R_{trp}$ via Eq.7. The transmitted total filament current, which is still coupled to the evolving upstream plasma density, is then recovered by plugging Eq.8 into Eq.6. It may seem contradictory that $n^R_{trp} = n^L_{trp} > 0$ in the limit of no trapped ions. But the trapped ion plasma does not exist because it has zero width and $P_{trp} = 0$. Its "density" is nonzero at just one radial point, equal to the expected electron density at the potential minimum of a SCL sheath without trapped ions. This scenario successfully reproduces the conventional SCL solution.

The concepts introduced here are adaptable to other geometries with minor changes. The trapped ion plasma's current enhancement effect discussed above increases from r_v/R_{ct} for a cylindrical geometry trapped ion plasma to ${r_v}^2/{R_{ct}}^2$ for spherical geometry. There is no enhancement for a fully planar discharge where the trapped ion plasma is also planar, as first argued in Ref.12. If the roles of the electrodes are reversed in curved geometry, meaning outer electrode is the negatively biased emitting cathode, a trapped ion plasma in a SCL sheath will interestingly cause a *reduction* of transmitted current due to contraction of the effective radius of the MSCL emission. We suggest that the contraction may play a role in the sheath physics of hot hollow cathode[37,38] devices.

E. Reducing the equation set to a solvable form

Using Equations 3-9 we can reduce the number of unknowns in the coupled differential Equations 1 and 2 to two variables - the downstream density of the trapped-ions plasma, n^L_{trp}, and the radial extent of the trapped-ions plasma r_v. One useful substitution needed in the process comes from Eq.8 as -

$$n^L_{ups}\, r_v = \frac{n^L_{trp}}{\beta} \tag{11}$$

where,

$$\beta = \frac{\alpha}{R_{ct}} \sqrt{\frac{\pi m_e}{2 k_B T_{emt}}} \tag{12}$$

Now using Eq.s 3,10, 11, and 12 we can express Eq. 1 in terms of n^L_{trp} and r_v as -

$$(R_{an}-r_v)\frac{dn^L_{trp}}{dt} - n^L_{trp}\frac{dr_v}{dt} = \frac{\Gamma_{emt}\beta}{2\pi n_{emt}} n^L_{trp}\left(1-\mathrm{e}^{-\frac{(R_{an}-r_v)}{\Delta_{iz}}}\right) - 2\sqrt{\frac{k_B T_e}{m_i}}\, n^L_{trp} \quad (13)$$

Using Eq.s 10,4, 11, and 12 we can express Eq.2 in terms of n^L_{trp} and r_v as -

$$R_{ct}\,(r_v-R_{ct})\frac{dn^L_{trp}}{dt} + R_{ct}\, n^L_{trp}\frac{dr_v}{dt} = \frac{n^L_{trp}}{\beta}\sqrt{\frac{k_B T_e}{m_i}}\left(1-\mathrm{e}^{-\frac{(r_v-R_{ct})}{\Delta_{cx}}}\right) - R_{ct}\sqrt{\frac{k_B T_i}{2\pi m_i}}\, n^L_{trp}\,\mathrm{e}^{\left(\frac{T_{emt}}{T_i}\ln\left(\frac{n^L_{trp}}{n_{emt}}\right)\right)} \quad (14)$$

The boxed Equations 13 and 14 form a system of coupled differential equations which can be solved numerically for n^L_{trp} and r_v, given their initial values. Mathematically, Equations 13 and 14 are Generalized Lotka-Volterra (GLV) equations with function-based interactions between the variables. Numerically, one can also solve Eq.13 and 14 as linear equations for $\frac{dn^L_{trp}}{dt}$ and $\frac{dr_v}{dt}$ and use forward difference with an adequately small time-step to evolve n^L_{trp} and r_v. Both methods yield convergent solutions. We adopted the faster linear equations method in our solutions using a time-step of $10^{-10}\,s$ which well resolves the sheath-dynamics time scale of $\sim 10^{-7}\,s$.

The choice of numerically solving differential equations in n^L_{trp} and r_v instead of P_{trp} and P_{ups} are as follows. In practical terms, the differential equations expressed terms of the P's contain singularities that complicate solving, and the upper bounds are not very clear. The r_v has clear bounds in both directions (the electrodes). Meanwhile, n^L_{trp} has physical nonzero bounds that establish clear limits for the solver. The minimum value of n^L_{trp} corresponding to a SCL sheath without trapped ions was discussed earlier. The maximum value of n^L_{trp} is n_{emt}, corresponding to when the inverse sheath vanishes. In this scenario, the trapped ion plasma has reached the cathode, fully neutralizing all available emitted electrons, allowing all of them into the upstream plasma. Any further accumulation of charge-exchange ions will cause a breakdown of neutrality, resulting in the "quenching instability" demonstrated in the simulation paper[19].

Quenching instabilities cause a rapid expulsion of many ions in the trapped ion plasma. The instability itself cannot be captured within this model which assumes the two plasmas are coupled and evolving in a quasistatic manner. Furthermore, the model equations break down when $n^L_{trp} > n_{emt}$ since Eq.6 suggests a transmitted electron current exceeding the maximum available emission. It is known from simulations that after a quenching instability, a quasi-steady TPM reforms with fewer trapped ions. This may be approximated in the model by reducing n^L_{trp} and r_v, which, due to the couplings in Eqs. 1–9, also implies that the properties of the upstream plasma must change post-instability. Determining the best way to set a post-quenching-instability TPM state consistent with the simulations and the model equations is left for future work.

We remark that if n^L_{trp} reaches n_{emt} *and* r_v reaches R_{ct}, the cathode is transmitting the full emitted current even without the help of trapped ions. This signifies a completed transition to the classical, temperature-limited sheath regime. Conversely, if r_v reaches R_{an}, the discharge has entered the AGM with no upstream plasma.

Now that we have derived and explained the model, the next step will be to numerically solve the equations 13 and 14 to model the evolution of an TPM in a cylindrical filament discharge.

F. A sample solution

We demonstrate a sample solution of Eq.s 13-14 ($\equiv$ Eqs. 1-9) in Fig.3 using the parameters of Table I which correspond to the simulated system in the simulation paper[19]. As seen in Table I the T_{emt} value of $0.5\,eV$ was chosen to be a few times higher than typical thermionic cathode temperatures to ensure adequate local Debye length resolution in the near-filament region of the simulation domain[19]. This choice helped manage computational cost in the simulations, as resolving the local Debye length becomes increasingly challenging at lower T_{emt} values. While this simplification may influence some details of the solution, it is not expected to alter the fundamental nature of the sheath physics under consideration.The initial values $n^L_{trp}(0)$ and $r_v(0)$, although arbitrary, are conceivable in the simulations. They represent the initial TPM profile that is chosen for the solver to clearly demonstrate the aid-compete effect.

TABLE I: Fixed parameters in the solution of Fig.3

Parameter	Value
n_{emt}	$2.29\times10^{16}\,m^{-3}$
Γ_{emt}	$1.0214 \times 10^{19}\,m^{-1}s^{-1}$
$n^L_{trp}(0)$ (initial value)	$7.5\times10^{15}\,m^{-3}$
$r_v(0)$ (initial value)	$0.34\,mm$
Δ_{cx}	$3.753\,mm$
Δ_{iz}	$0.997\,m$
T_{emt}	$0.5\,eV$
T_e	$2.843\,eV$
T_i	$0.132\,eV$
R_{ct}	$0.3\,mm$
R_{an}	$7.5\,mm$
Ions	Ar^+
α	$8.25\times10^5\,ms^{-1}$

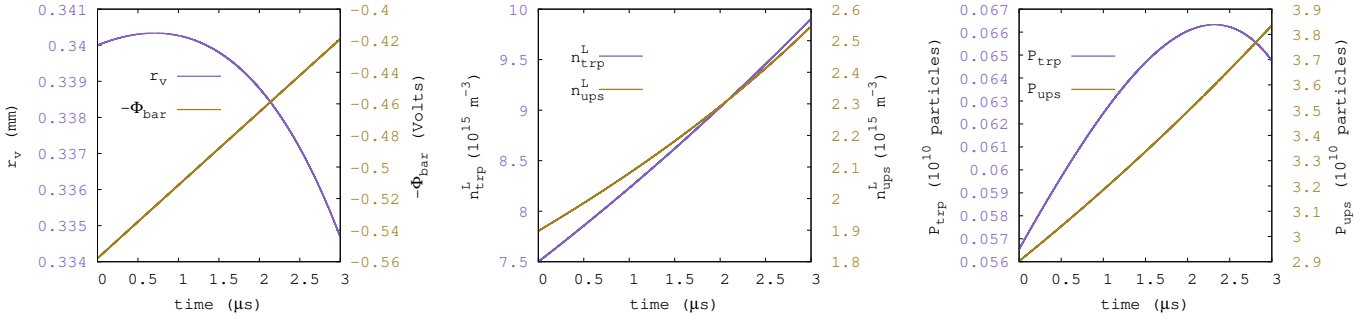

(a) $r_v(t)$ & $-\Phi_{bar}(t)$ (b) $n^L_{trp}(t)$ & $n^L_{ups}(t)$ (c) $P_{trp}(t)$ & $P_{ups}(t)$

FIG. 3: Sample solutions: Using the parameters of I Eq.s 13-14 are solved to yeild (a) dual plots of r_v and $-\Phi_{bar}$, (b) dual plots of n^l_{trp} and n^L_{ups}, and (c) dual plots of P_{trp} and P_{ups}.

In Fig.3 three pairs of solved variables are plotted as functions of time - Fig.3a plots the trapped-ion plasma's radial extent, r_v and the barrier potential, $-\Phi_{bar}$. Fig.3b plots n^L_{trp} and n^L_{ups}, the densities at the downstream edges of the trapped-ions plasma and the upstream plasma. Fig.3c plots P_{trp} and P_{ups}, the populations of the trapped-ions plasma and upstream plasma. The solutions are plotted for a $3\,\mu s$ time-interval.

We observe in Fig.3c that for the first 2.3 microseconds P_{trp} and P_{ups} have a mutually aided growth. After $2.3\,\mu s$ however, competitive effects become dominant and P_{trp} can been seen to fall while P_{ups} continues a monotonic rise. Generally we would expect the TIP radius r_v to rise and fall with the P_{trp}. However we observe in Fig.3a that although the r_v has a similar peaking and falling trend as P_{trp} its maximization point occurs much earlier at $0.75\,\mu s$. Hence, between $0.75\,\mu s$ and 2.3 the TIP layer is shrinking, yet its population is rising. Such a situation becomes possible owing to the ultra-slow movement of the r_v in this particular solution. In the $3\,\mu s$ plotted in Fig.3a, the r_v has only moved about $0.007\,mm$ in the $7.2\,mm$ electrode gap. Because of the ultra-slow contraction of the TIP, the charge-exchange probability in the TIP layer does not vary significantly. As such the 'aid'-part of the model can continue to sustain a rising P_{trp} until the 'compete'-part eventually takes over at $2.3\mu s$ as seen in Fig.3c. For a solution with a faster moving r_v having a similar shape as in Fig.3a, we can expect the maximization points of r_v and P_{trp} to be closer in time.

The densities on the downstream edges of the two plasmas plotted in Fig.3b grow nonlinearly through the $3\,\mu s$ period with the n^L_{trp} growing at a faster rate than n^L_{ups}. The rising of n^L_{trp} implies that the inverse sheath is getting weaker. This effect is also evident from the diminishing magnitude the barrier potential, $-\Phi_{bar}$ in Fig.3a.

The solution in Fig.3 exemplifies some of the complexities of the aid-compete dynamics. For example, inverse sheath can continue to get weaker even as the total trapped-ions population decreases. This can happen when the upstream plasma is gaining population as in the P_{ups} of Fig.3c and also expanding towards the cathode as in the r_v of Fig.3a. In this situation the inverse sheath is getting weaker, not due to ions getting trapped in the VC, but because it is transiting to a classical sheath.

III. VERIFICATION OF THE MODEL USING SIMULATIONS

Next, we test our analytical aid-compete model using simulations. The simulations are performed using the code and set-up of the simulation paper[19], their device parameters following Table I except for the initial values $n^L_{trp}(0)$ and $r_v(0)$, and the collision mean free paths Δ_{cx}, and Δ_{iz}. The $n^L_{trp}(0)$ and $r_v(0)$ correspond to a chosen TPM snapshot from Ref.[19] simulation, while Δ_{cx}, and Δ_{iz} are varied parameters in these tests.

A. Test-1: Variation of the charge exchange collision frequency

The initial plasma profile for the analytical solutions and simulations of this paper is a mid-simulation profile from one of the numerical experiments of Ref. [19]. Specifically, it is a TPM profile formed 156 microseconds into the simulation. The TIP in this profile has a downstream quasi-neutral density, $n^L_{trp} \approx 2.0\times10^{16}\,m^{-3}$ and a radial extent, $r_v \approx 0.52\,mm$. These values are fed as the initial values $n^L_{trp}(0)$ and $r_v(0)$ for the analytical equations' solver and a set of solutions are obtained for a fixed ionization mean-free-path (mfp), $\Delta_{iz} = 2.25\,m$, and a variable charge exchange mfp given as $\Delta_{cx} = f \times 3.73\,mm$, where $0.2 \le f \le 1.8$. The fixed Δ_{iz} and the base value for the Δ_{cx} variation i.e. $\Delta_{cx} = 3.73\,mm$, are estimated from the given initial profile. The goal of the experiment is to demonstrate how the aid-compete solutions vary with increased / decreased rates of ion-trapping through Δ_{cx}.

The first row of Fig.4 plots the solutions for a color coded f. The solved r_v, P_{trp}, and P_{ups} are plotted in Fig.4a,b, and c respectively. A larger f implies a longer charge exchange mfp hence a lower rate of such collisions. In Fig.4a and b the nonlinear increase r_v and P_{trp} for all values of f can be attributed

to the fed initial values $n^L_{trp}(0)$ and $r_v(0)$. The rates of ascent of r_v and P_{trp} vary with f, rising faster for lower values of f. A lower f implies more charge-exchange collisions which accelerates the process of ion trapping. Hence in Fig.4a and b the r_v and P_{trp} grow faster for lower f.

The initial conditions are such that the interaction between the two plasmas is more competitive than aiding, favoring the radial expansion of the TIP. Hence the P_{trp} in Fig.4b grows at the expense of the corresponding P_{ups} in Fig.4c for all values of f. For higher f values in Fig.4c the P_{ups} curve descends slower. This is because the higher f values ($\equiv$ less charge exchanges) slow down the competitive growth of P_{trp} in Fig.4b.

We seek to investigate an equivalent variation of the charge exchange collision rate using simulations. In order to set up an equivalent set of simulations, we continue the numerical experiment of Ref.[19] from the $156\,\mu s$ point as a set of branched simulations with systematically scaled charge-exchange cross-sections.

Note that unlike the model, the charge exchange cross-section in simulation, $\sigma_{cx}(E_i)$ is a dynamic quantity that depends on the energy, E_i of individual ions at each time-step. Nevertheless, we can still apply a gross variation of the charge-exchange cross-section over the entire ion population throughout the simulation using a modified value, $\sigma^{mod}_{cx}(E_i) = f \times \sigma_{cx}(E_i)$. The factor f allows an enveloping external control over the charge-exchange frequency of the system while keeping $\sigma_{cx}(E_i)$ energy-dependent and temporally dynamic. The simulation time step is $5 \times 10^{-12}\,s$, which is much smaller than the model solver's time step ($1 \times 10^{-10}\,s$). This difference is expected since the simulation time step is constrained by PIC resolution requirements[19], whereas the model solver is not.

The simulation results using modified charge exchange cross-sections are plotted in the second row of Fig.4 with the measured r_v, P_{trp} and P_{ups} plotted in Fig.4d, e, and f respectively. Note that there is a role reversal of the scaling factor f between Fig.4a-c and Fig.4d-f. In the model equations' solutions the f scales Δ_{cx} while in the simulations the f scales $\sigma_{cx} \sim 1/\Delta_{cx}$. Notwithstanding the role reversal of f the color code used in Fig.4d-f matches that of Fig.4a-c : *As one moves from red to violet the charge exchange frequency increases in both sets.*

In Fig.4d the $r_v(t)$ from simulation is measured using the method outlined in Ref.[19]. The $P_{trp}(t)$ and $P_{ups}(t)$ in Fig.4e-f are counts of the number of ions downstream and upstream of the measured $r_v(t)$ respectively. These counts unavoidably absorb ions occupying the sheath regions.

Comparing Fig.4a with Fig.4d we find that while the theory plot shows an increasing rate of growth of r_v with increased charge exchange collisionality, the simulation r_v's do not show any specific trend with the change in charge exchange collision frequency. Moreover unlike the theory plots, some of the r_v curves from the simulation show strong undulations, being affected by quenching instabilities. For example, see the $f = 0.25$ curve in Fig.4d. Comparing Fig.4b with Fig.4e we find that there is gross agreement between the two sets of curves in the fact that both exhibit faster growth of P_{trp} with increased charge exchange collision frequency. Comparing Fig.4c with Fig.4f we find a discrepancy in the scaling of P_{ups} with charge-exchange frequency between the simulations and the model. While more charge-exchange collisions leads to faster decrease of P_{ups} in the model (see Fig.4c), the simulations, as per Fig.4f, are showing that P_{ups} decreases slower for higher charge exchange frequency.

We note that there is a qualitative dissimilarity of the simulations' r_v plots (Fig.4d) from the model (Fig.4a) in not showing a trend with variation of the charge exchange frequency. Also, the variation of simulations' P_{ups} with charge exchange frequency (Fig.4e) has the reverse trend to that of the model (Fig.4c). Both these discrepancies between the model and the simulations can be resolved to some extent, when we consider the difference in the spatial extent of the effect of scaled charge-exchange collisions between the model and the simulations.

In the model the charge exchange collisions are only considered in the trapped-ions plasma layer, while in the simulation the charge-exchanges happen through out the domain including the upstream plasma, where unaccelerated 'cold' ions have more charge-exchange collisions with neutrals than the accelerated ions entering the VC. The difference in collisionality arises from the larger charge exchange cross-sections of colder ions with cold neutrals (see Fig. 5 of Ref. 32). It is possible that raising the charge exchange collision rate in the entire domain of the simulation produces a stronger drag on the ion transport in the upstream plasma suppressing its decay. This drag may be having a stronger effect on P_{ups} over the competition from the increasing P_{trap} resulting in the anomaly of scaling with collision frequency in Fig.4f. The same drag could also be preventing a trend with charge exchange collisionality from emerging in the simulations' r_v curves.

We tested this hypothesis by limiting the scaled charge exchange cross-section, σ^{mod}_{cx} to the region downstream of $r_v(t)$ while the rest of the domain maintained the unmodified σ_{cx}. The results with the spatially adjusted σ_{cx} are shown in the third row of Fig.4g-i where r_v, P_{trp}, and P_{ups} are plotted in Fig.4g, h, and i respectively.

The simulations with the spatially varied charge-exchange collisionality demonstrate a greater level of agreement with the model's data. Comparing Fig.4a with Fig.4g we find that the r_v's in both sets show an increased rate of growth with increased charge exchange frequency. The discrepancy of the P_{ups} trend observed in Fig.4f is also resolved in Fig.4i. Now, both Fig.4c and 4i show a faster rate of fall of P_{ups} with increased rate of charge exchange in the TIP. Fig.4g-i demonstrates the importance of the neutral drag forces (on ions) in the aid-compete effect and it is something to be considered in future improvements to the theory model.

Overall the set of numerical experiments in Fig.4 demonstrate that indeed there is an aid-compete effect at work in a TPM, and verify the correctness in our mathematical approach towards modeling this effect.

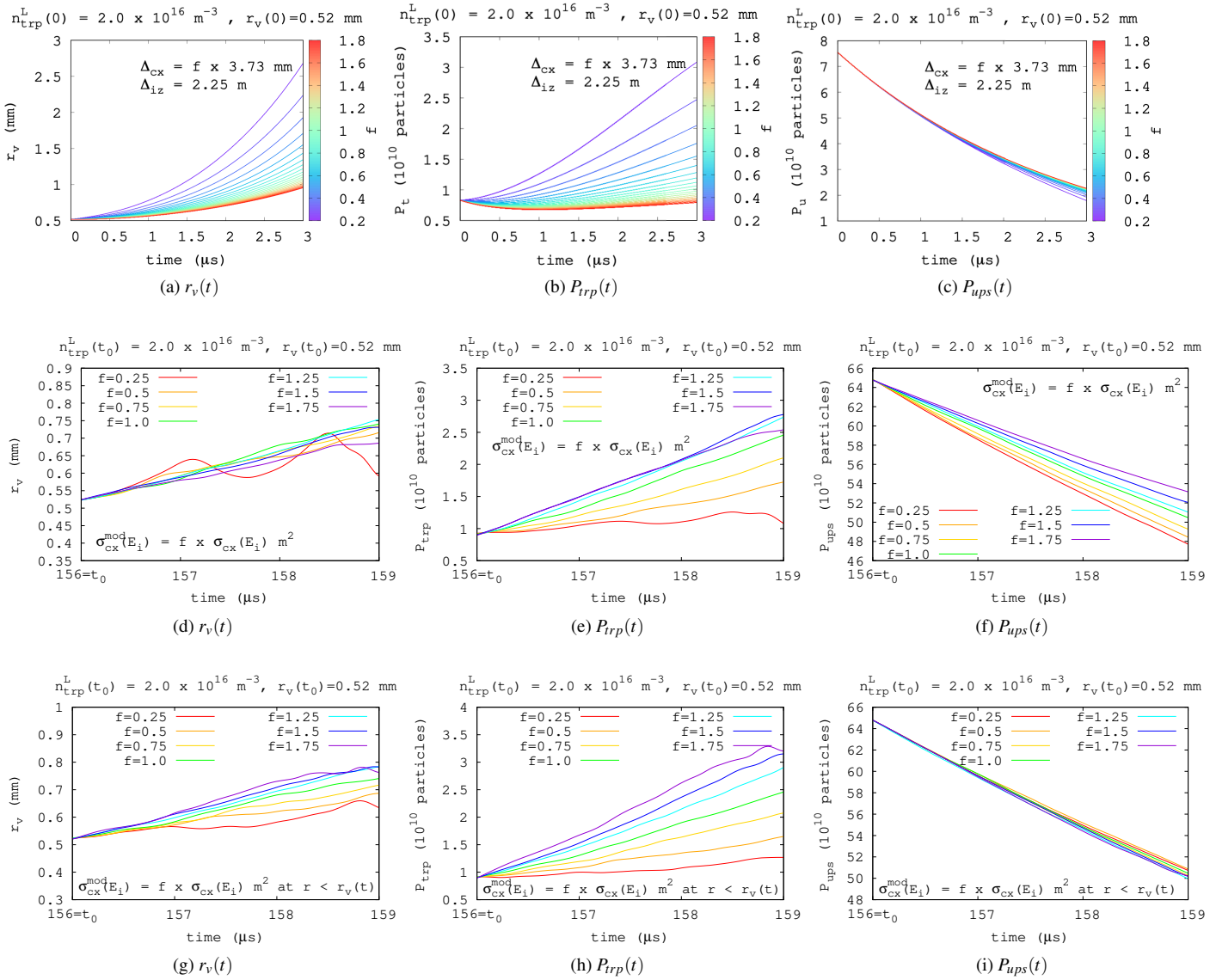

FIG. 4: Comparing the analytical model with simulations for a systematic variation of charge exchange collision frequency. Top row shows the model's solution for a variation of charge exchange mean free path, Δ_{cx}. Middle row shows the simulation solution for an equivalent variation of the charge exchange cross-section, $\sigma_{cx}(E_i)$ where E_i is ion energy. Bottom row shows the simulation solution for charge exchange cross-section varied only within the trapped-ions layer i.e. in the $r < r_v$ region. In each row the solutions for three quantities are shown. First-column panels i.e. (a),(d), and (g) show the solution for r_v. Second-column panels i.e. (b), (e), and (h) show the solutions for P_{trp}. Third-column panels i.e. (c), (f), and (i) show the solutions for P_{ups}. Variation of the charge exchange frequency is achieved through the multiplicative factor f given in the color-bar or key of the panel.

B. Test-2: Variation of the neutral pressure

We ran a second test to verify the model using simulations, this time scaling the background pressure so that both Δ_{cx} and Δ_{iz} are varied concurrently as would happen in experiments. The results are illustrated in Fig.5. The first row, Fig.5a-c, depicts the solutions of the analytical model while the the second row, Fig.5d-f depicts the simulation results. The third row, Fig.5g-i depicts a second set of analytical solutions obtained with identical conditions as the first row except for a slightly higher upstream plasma potential Φ_{up}, affecting the Δ_{cx} and Δ_{iz}. The starting profile and the fixed system parameters are the same as in Test-1 (Fig.4) and so is the arrangement of the plotted solved variables viz., r_v, P_{trp}, and P_{ups}. The background neutral pressure, Π_{neu} at room temperature, $300K$ is varied as $\Pi_{neu} = f \times 25 mTorr$ where $0.2 \leq f \leq 1.8$.

For the given initial values, $n^L_{trp}(0)$ and $r_v(0)$, Fig.5a and b reveal the r_v and P_{trp} to be increasing functions with time. The rate of their growth increases with an increase in the neutral pressure. The set of P_{ups} in Fig.5c are all decreasing with time

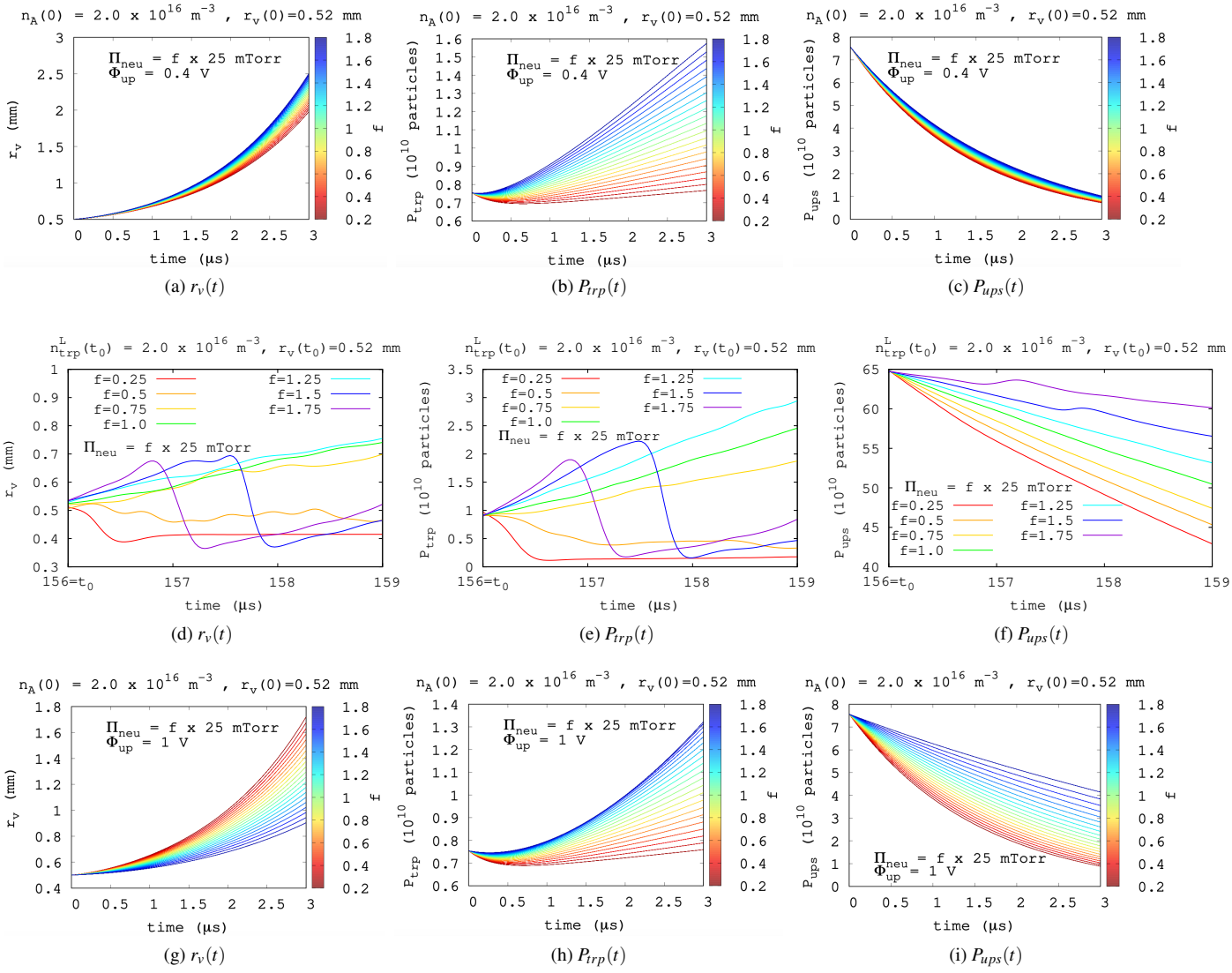

FIG. 5: Comparing the analytical and simulation solutions for a systematic scaling of the neutral density: Top row, (a) – (c) shows the model's solutions while the middle row, (d) – (f) shows the simulation solutions. Bottom row, (g) – (i) shows a second set of analytical solutions obtained assuming a slightly higher (by $0.6V$) upstream plasma potential than the first row's solutions. In each row, the first-column panels viz (a), (d), (g) shows the r_v solution, the second-column panels viz (b), (e), (h) show the P_{trp} solution, and the third-column panels viz (c), (f), (i) show the P_{ups} solution. Variation of the neutral pressure is achieved through factor f shown in the color-bar or key of the panels.

at rates which become slower with increasing neutral pressure. This can be understood by considering the effects of the changing neutral pressure on charge exchange and ionization collision rates. While the growth of r_v and P_{trp} are accelerated by increased charge exchange collisions rate at higher pressures, the corresponding decline of P_{ups} via the 'compete' effect gets slowed down at higher pressures due to an increase in the upstream ionization rate.

In Fig.5d-f corresponding evolution of the r_v, P_{trp}, and P_{ups} functions from equivalent simulations are depicted. Coarsely, the characteristics of Fig.5d-f are convergent with those of Fig.5a-c. The r_v and P_{trp} curves at the highest pressures in Fig.5d and e are affected by quenching instabilities producing strong undulations; see $f = 1.5$ and $f = 1.75$ curves in Fig.5d-e. For these curves, their trend prior to the instability needs to be considered. We observe that that the P_{ups} curves from the simulations (Fig.5f) are significantly more divergent with the changing f than the corresponding P_{ups} curves form the model (Fig.5c).

Now, the Δ_{cx} and Δ_{iz} in the solutions of Fig.5a-c were calculated assuming an upstream plasma potential, ($\sim$ the anode sheath voltage) $\Phi_{up} = 0.4V$; see Fig.1. While this is a good approximation for the upstream plasma potential in the initial profile adopted from the snapshot of Ref.[19], we have seen in simulations that the upstream plasma potential can vary spatially as well as temporally within a range of $\sim 1V$.

Out of curiosity, we tested what would happen to the solutions of Fig.5a-c if we just raised the assumed upstream plasma potential from $0.4V$ to $1.0V$. The results are depicted in Fig.5g-i. Interestingly in Fig.5g, the growth rate of r_v decreases with increased neutral pressure, the opposite of what we observed in Fig.5a. This is most likely due to a stronger influence of upstream ionization at the higher value of upstream plasma potential. Also, we observe that the P_{ups} curves are significantly more spread out in the f space, similar to the simulations' P_{ups} in Fig.5f.

The results of Fig.5a-i, while demonstrating agreement of the model with simulations, also highlight some of the intricacies of the aid-compete model, especially how minor changes to one or more parameters can substantially alter the outcome. Similar conclusions were arrived at in Ref.[19] where we demonstrated the heightened sensitivity of the system to ambient changes, when operated near its ionization threshold.

C. Behavior of the model after r_v reaches one of the electrodes

Finally, let us focus on the physical limits of the analytical model. Although the model treats a discharge in the TPM, it can demonstrate the transition to the TLM (classical sheath mode), AGM (inverse sheath mode) or LM (SCL sheath mode). Enhancements would be needed to accurately advance the discharge that enters the latter three modes. In the model's current form, the upstream ionization rate and downstream ion trapping rate both vanish if the corresponding plasma's length reaches zero. In a real AGM, there is still ionization in a thin region of the anode sheath where the potential exceeds the ionization threshold. Similarly, if the discharge has a SCL sheath with no trapped ions, there is still a finite length potential well where trapped ions could start accumulating. These regions could be accounted for by adding a suitable length to the regions of ion creation in Eqs. 1,2. In Eq. 1, the exponential factor would be -(R_{an} -r_v +Δ_r)/Δ_{iz} for some Δ_r expression. Calculating Δ_r is nontrivial because it is a function of the existing discharge state and depends on the details of the potential distribution in the space charge regions, so it is left to future work. A useful benefit of including a Δ_r is that it would enable the formation of a TPM with an upstream plasma even when there is only one plasma in an AGM initially. This is likely to happen in practice when an initial AGM discharge is subjected to an increase of bias or neutral pressure.

The end of the TPM and onset of other modes occurs when r_v reaches an electrode. Fig.6 shows solutions for a transition to an AGM. Fig.6a plots n^L_{trp} and n^L_{ups}, Fig.6b plots r_v and $-\Phi_{bar}$, and Fig.6c plots P_{trp} and P_{ups}. We see that the r_v hits the R_{an} at about $3\,\mu s$. At this time there is no more upstream plasma ($P_{ups} = 0$) even though there remains a small non-zero n^L_{ups} due to its coupling to the downstream plasma seen in Eq. 7,8, as shown by the dashed lines in Fig.6a. This n^L_{ups} produces a persisting source of ion-trapping in Eq. 2 even after upstream plasma is lost. However due to its small value once $P_{ups} = 0$ is reached this unphysical n_{ups} only produces a quantitative 'error' on the net loss rate of P_{trp} once r_v hits R_{an} in Fig.6c. This is because Eq. 2 is dominated by the loss term in the RHS which is physical.

In Fig.6b, we did not fix $r_v = R_{an}$ beyond $3\,\mu s$. We let the solver continue to evolve r_v but enforced the condition $r_v = R_{an}$ only if the solved r_v became greater than R_{an}. Implementing the limit this way leaves the r_v free to fall below R_{an} if the solver took it in that direction. However we found that r_v stayed that R_{an} implying AGM. Trapped ions continue leaking to the cathode, causing P_{trp} and n^L_{trp} to decay in time. The barrier potential $|\Phi_{bar}|$ continues to increase because it enforces neutrality of the remaining trapped ion plasma by restricting how many thermoelectrons can enter. A true steady state AGM is not reached because there is no production of new trapped ions in the model once the upstream plasma feeding it is eliminated. In Fig.6c the P_{ups} hits zero as soon as r_v reaches R_{an}.

Now let us look at the solutions when r_v reaches the opposite limit, R_{ct}. As before, the solutions are plotted in pairs n^L_{trp} and n^L_{ups} in Fig.7a, r_v and $-\Phi_{bar}$ in Fig.7b, and P_{trp} and P_{ups} in Fig.7c. In Fig.7b the r_v hits R_{ct} at about $2.3\,\mu s$. Again, here we do not hold r_v at R_{ct} once it hits, only enforcing it to not fall any further.

Once r_v reaches R_{ct} at $2.3\,\mu s$, the trapped ion plasma has been fully expelled to the cathode and P_{trp} hits zero simultaneously as expected. Afterward, n^L_{trp} still has a nonzero value. As predicted earlier, the model is capturing a realistic scenario called the Langmuir mode (LM) where the cathode has a conventional SCL sheath with no finite-length trapped ion plasma. It is equivalent to declare that a quasineutral trapped ion plasma is present at one point, the potential minimum of the virtual cathode. The value of n^L_{trp} thus equally represents the density of emitted electrons at the minimum, which correspondingly determines the SCL current projected into the upstream plasma. The barrier potential $-\Phi_{bar}$ in Fig.7b remains nonzero to regulate the SCL emission. It is known that the SCL current density is proportional to the upstream plasma density n^L_{ups} which is continuing to increase in time. The system enters the classical TLM when n^L_{trp} reaches n_{emt} and simultaneously $-\Phi_{bar}$ reaches zero. The numerical continuation of the solution where $n^L_{trp} > n_{emt}$ is unphysical because the cathode cannot emit any more electrons. A TLM is incompatible with our model equations, but it could easily be modelled with a simpler set of equations containing just one (upstream) plasma and a fixed value of $\Gamma_{tmt} = \Gamma_{emt}$.

IV. CONCLUSION

In this paper, we demonstrated an approximate analytical model for the dynamical coupling between the upstream and downstream plasmas in the two plasma mode of a cylindrical single-filament discharge. The model is aptly named the aid-and-compete model as it essentially provides a proof-of-principle for the mutually enhancing and opposing effects at play between the two plasmas.

Formulated in axisymmetric cylindrical geometry, the model's generalized form, expressed through Eq.s 1-14,

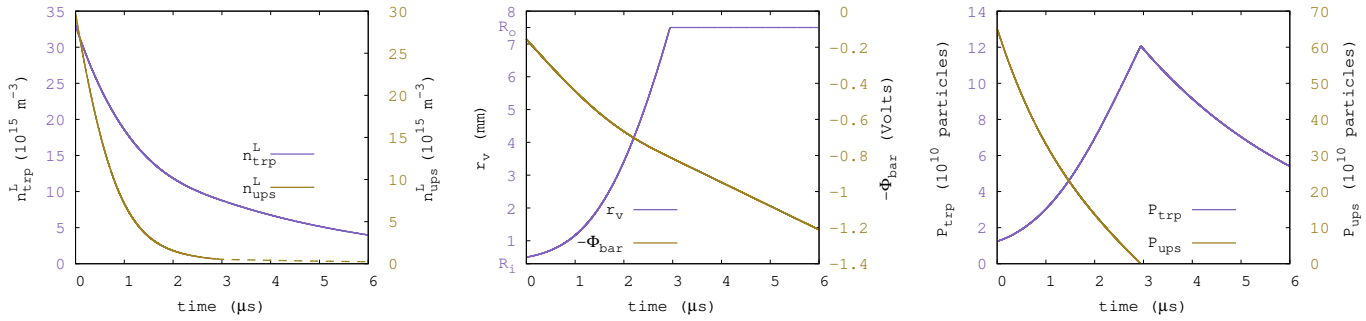

(a) $n^L_{trp}(t)$ & $n^L_{ups}(t)$ (b) $r_v(t)$ & $-\Phi_{bar}(t)$ (c) $P_{trp}(t)$ & $P_{ups}(t)$

FIG. 6: Sample demonstration of how the solution behaves after r_v, through Eq.s 13-14, expands upto the anode at R_{an}. Once r_v hits R_{an} there is only one plasma, the trapped-ions plasma in the system. (a) shows the solution for downstream densities of the trapped-ions layer, n^L_{trp} and the upstream layer, n^L_{ups} (b) shows the solution for the trapped-ions radius r_v and the barrier potential Φ_{bar}. (c) shows the solutions for the downstream and upstream densities P_{trp} and P_{ups}. Dotted segments in the panels indicate non-physical values.

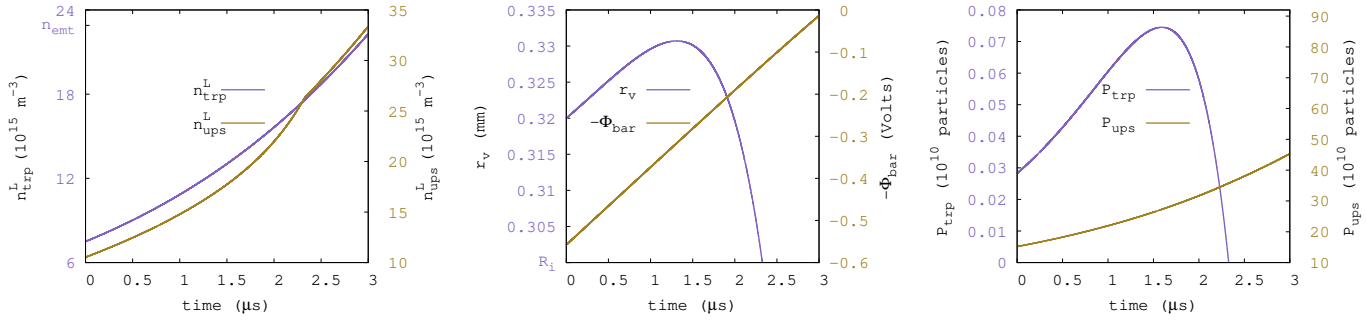

(a) $n^L_{trp}(t)$ & $n^L_{ups}(t)$ (b) $r_v(t)$ & $-\Phi_{bar}(t)$ (c) $P_{trp}(t)$ & $P_{ups}(t)$

FIG. 7: Sample demonstration of how the solution behaves after r_v, through Eq.s 13-14, shrinks to cathode radius, R_{ct}. Once r_v hits R_{ct} there is only one plasma, the upstream plasma in the system. (a) shows the solution for downstream densities of the trapped-ions layer, n^L_{trp} and the upstream layer, n^L_{ups} (b) shows the solution for the trapped-ions radius r_v and the barrier potential Φ_{bar}. (c) shows the solutions for the downstream and upstream densities P_{trp} and P_{ups}.

works for any annular aspect ratio of a co-axial discharge having the same polarity i.e. an inner emitting cathode. Numerical solutions of the model, with systematically varied mean free paths of charge-exchange and ionization collisions, demonstrate a behavior consistent with physical intuition. These solutions are further corroborated by simulations conducted under equivalent conditions.

Our model of the two plasma coupling is approximate and somewhat qualitative. It captures the collision-driven and collisionless mechanisms that constitute the aid-compete effect, such as (i) how the rate of ion trapping in the virtual cathode modulates the transmitted electron flux that causes ionization upstream, and (ii) the transport of ions from the upstream plasma modulating the rate of ion trapping in the potential well. While the model has still been successful at predicting general direction of evolution of the system in simulations, various secondary effects neglected in the model can introduce quantitative discrepancies.

For example, a major mode transition was seen in one of the simulations of Ref.[19] the globally averaged density of plasma collapsed by an order-of-magnitude due to a $1\,V$ drop in the anode sheath voltage. Although the anode sheath voltage is weak, it increases the double layer voltage further beyond the applied bias which makes a substantial difference when operating near the gas ionization threshold. A useful extension of the model would thus be to calculate the anode sheath's voltage in terms of the discharge state and include its effect on Δ_{iz}. In the present paper's calculations, the ionization mean free path Δ_{iz} was held fixed (independent of electron energy and time).

Other secondary effects include finite sheath widths, curved geometry effects on sheath physics (e.g. orbital motion of ions near the cathode), collisional drag slowing the transport of upstream ions, and presheath's influence on the upstream plasma's potential and density distributions. The analytical model's quantitative agreement with simulations or even experiments can be improved via a system-specific inclusion of important secondary effects in the equations. For example, the

collisional effects impeding the electron and ion flows could be empirically or analytically integrated into Eq.s 1 and 2. The model could also take into account corrections accounting for the sheath widths, the most important being the double layer which is known from simulations to take up a substantial portion of the electrode gap and reduce the space available to the plasmas. Calculations of ionization and ion trapping rates should be extended to include the amount that occurs in the space charge regions. This amount is a minor correction in an existing TPM but becomes crucial when aiming to advance a discharge state starting in the single-plasma mode, namely AGM or LM.

Including more of the effects mentioned above will complicate the original equations (Eq. 1-9) by adding additional couplings among them. This could inhibit the substitutions that we invoked to reduce the equations down to two (Eq. 13,14). Nevertheless, the more entangled equations would still be numerically solvable, with extra care needed to avoid numerical transitions to unphysical values.

As a secondary outcome, we discussed the broader applicability of the theoretical model for MSCL sheaths[16] in calculating currents across double layers, as opposed to relying on the Langmuir condition[35]. We note that a double layer naturally forms an MSCL sheath on its lower potential side, where it transitions into the flat potential of the downstream quasineutral layer, making the MSCL sheath theory relevant.

Now that the consequences of the finite-length quasineutral trapped ion plasma have been clearly demonstrated both in analytical calculations and kinetic simulations of filament discharges, future work is encouraged to advance these models and develop experimental diagnostic methods for direct measurement of trapped ion plasmas near hot cathodes.

ACKNOWLEDGMENTS

This work was performed under the auspices of the U.S. Department of Energy by Lawrence Livermore National Laboratory under contract DE-AC52-07NA27344. Authors thank Z. Idema for useful discussions.

DATA AVAILABILITY STATEMENT

The data that support the findings of this study are available from the corresponding author upon reasonable request.

[1]X. Li, H. Wu, Y. Zhong, C. Guo, L. Yi, W. Jiang, and Y. Zhang, J. Phys. D Appl. Phys. **56**, 175202 (2023).
[2]E. Bogdanov, V. I. Demidov, I. D. Kaganovich, M. E. Koepke, and A. A. Kudryavtsev, Phys. Plasmas **20**, 101605 (2013).
[3]Y. Zhong, H. Wu, X. Li, J. Gao, W. Jiang, Y. Zhang, and G. Lapenta, J. Phys. D Appl. Phys. **55**, 215203 (2022).
[4]L. S. Volkov, N. Y. Babaeva, and N. N. Antonov, J. Phys. D Appl. Phys. **54**, 105202 (2021).
[5]T. D. Akhmetov, V. I. Davydenko, A. A. Ivanov, and G. I. Shulzhenko, Plasma Fusion Res. **14**, 2406004 (2019).
[6]S. Jin, M. J. Poulos, B. Van Compernolle, and G. J. Morales, Phys. Plasmas **26**, 022105 (2019).
[7]D. Jiang, C.-S. Yip, W. Zhang, C.-Y. Jin, G.-S. Xu, and L. Wang, Rev. Sci. Instrum. **92**, 123503 (2021).
[8]V. Nemchinsky, IEEE Trans. Plasma Sci. IEEE Nucl. Plasma Sci. Soc. **42**, 199 (2014).
[9]T. Klinger, F. Greiner, A. Rohde, and A. Piel, Phys. Plasmas **2**, 1822 (1995).
[10]L. Malter, O. Johnson, and W. M. Webster, RCA Rev. **12**, 415 (1951).
[11]F. Greiner, T. Klinger, and A. Piel, Phys. Plasmas **2**, 1810 (1995).
[12]M. D. Campanell and M. V. Umansky, Plasma Sources Sci. Technol. **26**, 124002 (2017).
[13]H. J. Lee and J. K. Lee, Phys. Plasmas **5**, 2878 (1998).
[14]J. L. Lawless and S. H. Lam, J. Appl. Phys. **59**, 1875 (1986).
[15]O. Biblarz and W. J. Bell, IEEE Trans. Ind. Appl. **34**, 325 (1998).
[16]S. Takamura, N. Ohno, M. Y. Ye, and T. Kuwabara, Contrib. Plasma Phys. **44**, 126 (2004).
[17]G. R. Johnson and M. D. Campanell, Plasma Sources Sci. Technol. **30**, 015003 (2021).
[18]C.-S. Yip, C. Jin, W. Zhang, D. Jiang, and G. S. Xu, Phys. Scr. **98**, 025012 (2023).
[19]M. Sengupta and M. Campanell, "Sheath transitions in a cylindrical filament discharge: Axisymmetric 1D3V PIC-MCC simulations," In Communication.
[20]T. Klinger, F. Greiner, A. Rohde, and A. Piel, Phys. Plasmas **2**, 1822 (1995).
[21]S. Langendorf and M. Walker, J. Appl. Phys. **119**, 113305 (2016).
[22]I. V. Schweigert, Phys. Rev. Lett. **92**, 155001 (2004).
[23]J. Schulze, Z. Donkó, B. G. Heil, D. Luggenhölscher, T. Mussenbrock, R. P. Brinkmann, and U. Czarnetzki, J. Phys. D Appl. Phys. **41**, 105214 (2008).
[24]J. Schulze, A. Derzsi, K. Dittmann, T. Hemke, J. Meichsner, and Z. Donkó, Phys. Rev. Lett. **107**, 275001 (2011).
[25]D. Bhattacharjee, D. Jigdung, N. Buzarbaruah, S. R. Mohanty, and H. Bailung, Phys. Plasmas **26**, 073514 (2019).
[26]N. V. Landl, Y. D. Korolev, V. G. Geyman, O. B. Frants, I. A. Shemyakin, V. S. Kasyanov, I. V. Lopatin, and S. S. Kovalskii, Russ. Phys. J. **62**, 2024 (2020).
[27]X. Wang, J. Pilewskie, H.-W. Hsu, and M. Horányi, Geophys. Res. Lett. **43**, 525 (2016).
[28]B. Song, N. D'Angelo, and R. L. Merlino, J. Phys. D Appl. Phys. **25**, 938 (1992).
[29]S. D. Baalrud, B. Longmier, and N. Hershkowitz, Plasma Sources Sci. Technol. **18**, 035002 (2009).
[30]B. Scheiner, L. Beving, and S. D. Baalrud, Phys. Plasmas **26**, 013509 (2019).
[31]G. R. Johnson and M. D. Campanell, Plasma Sources Sci. Technol. **30**, 015003 (2021).
[32]V. Vahedi and M. Surendra, Comput. Phys. Commun. **87**, 179 (1995).
[33]M. Surendra, D. B. Graves, and G. M. Jellum, Phys. Rev. A **41**, 1112 (1990).
[34]W. H. Cramer, J. Chem. Phys. **30**, 641 (1959).
[35]Block, L.P. and Kungliga Tekniska Hoegskolan, Stockholm (Sweden). Institutionen foer Plasmafysik, (1972).
[36]L. P. Block, Astrophys. Space Sci. **55**, 59 (1978).
[37]D. Pedrini, R. Albertoni, F. Paganucci, and M. Andrenucci, IEEE Trans. Plasma Sci. IEEE Nucl. Plasma Sci. Soc. **43**, 209 (2015).
[38]R. Albertoni, D. Pedrini, F. Paganucci, and M. Andrenucci, IEEE Trans. Plasma Sci. IEEE Nucl. Plasma Sci. Soc. **41**, 1731 (2013).